



**HAL**  
open science

## **Frit inlet field-flow fractionation techniques for the characterization of polyion complex self-assemblies**

Ugo Till, Mireille Gaucher, Baptiste Amouroux, Stéphane Gineste, Barbara Lonetti, Jean-Daniel Marty, Christophe Mingotaud, Carmen R.M. Bria, S. Kim Ratanathanawongs Williams, Frédéric Violleau, et al.

### ► To cite this version:

Ugo Till, Mireille Gaucher, Baptiste Amouroux, Stéphane Gineste, Barbara Lonetti, et al.. Frit inlet field-flow fractionation techniques for the characterization of polyion complex self-assemblies. *Journal of Chromatography A*, 2017, 1481, pp.101-110. 10.1016/j.chroma.2016.12.050 . hal-01595439

**HAL Id: hal-01595439**

**<https://hal.science/hal-01595439>**

Submitted on 27 Nov 2019

**HAL** is a multi-disciplinary open access archive for the deposit and dissemination of scientific research documents, whether they are published or not. The documents may come from teaching and research institutions in France or abroad, or from public or private research centers.

L'archive ouverte pluridisciplinaire **HAL**, est destinée au dépôt et à la diffusion de documents scientifiques de niveau recherche, publiés ou non, émanant des établissements d'enseignement et de recherche français ou étrangers, des laboratoires publics ou privés.



## Open Archive Toulouse Archive Ouverte (OATAO)

OATAO is an open access repository that collects the work of Toulouse researchers and makes it freely available over the web where possible

This is an author's version published in: <http://oatao.univ-toulouse.fr/25142>

**Official URL:** <https://doi.org/10.1016/j.chroma.2016.12.050>

### **To cite this version:**

Till, Ugo and Gaucher, Mireille and Amouroux, Baptiste and Gineste, Stéphane and Lonetti, Barbara and Marty, Jean-Daniel and Mingotaud, Christophe and Bria, Carmen R.M. and Williams, S. Kim Ratanathanawongs and Violleau, Frédéric and Mingotaud, Anne-Françoise *Frit inlet field-flow fractionation techniques for the characterization of polyion complex self-assemblies*. (2017) Journal of Chromatography A, 1481. 101-110. ISSN 0021-9673

Any correspondence concerning this service should be sent to the repository administrator: [tech-oatao@listes-diff.inp-toulouse.fr](mailto:tech-oatao@listes-diff.inp-toulouse.fr)

# Frit inlet field-flow fractionation techniques for the characterization of polyion complex self-assemblies

Ugo Till<sup>a,b</sup>, Mireille Gaucher<sup>b</sup>, Baptiste Amouroux<sup>a</sup>, Stéphane Gineste<sup>a</sup>, Barbara Lonetti<sup>a</sup>, Jean-Daniel Marty<sup>a</sup>, Christophe Mingotaud<sup>a</sup>, Carmen R.M. Bria<sup>c</sup>, S. Kim Ratanathanawongs Williams<sup>c</sup>, Frédéric Violleau<sup>d,\*</sup>, Anne-Françoise Mingotaud<sup>a,\*</sup>

<sup>a</sup> Laboratoire des IMRCP, Université de Toulouse, CNRS UMR 5623, Université Paul Sabatier, 118 route de Narbonne, F-31062, Toulouse Cedex 9, France

<sup>b</sup> Département Sciences Agronomiques et Agroalimentaires, Université de Toulouse, INP-EI PURPAN, 75 voie du TOEC, BP 57611, F-31076 Toulouse Cedex 03, France

<sup>c</sup> Laboratory for Advanced Separations Technologies, Department of Chemistry, Colorado School of Mines, Golden, CO 80401, USA

<sup>d</sup> Laboratoire de Chimie Agro-industrielle (LCA), Université de Toulouse, INRA, INPT, INP-EI PURPAN, Toulouse, France

## ARTICLE INFO

### Keywords:

Flow field-flow fractionation  
Frit inlet flow field-flow fractionation  
Polyion complex micelles  
Polymers  
Self-assembly

## ABSTRACT

Polymer self-assemblies joining oppositely charged chains, known as polyion complexes (PICs), have been formed using poly(ethyleneoxide – b – acrylic acid)/poly(L-lysine), poly(ethyleneoxide-b-acrylic acid)/dendrigraft poly(L-lysine) and poly[(3-acrylamidopropyl) trimethylammonium chloride – b – N – isopropyl acrylamide]/poly(acrylic acid). The self-assemblies have been first characterized in batch by Dynamic Light Scattering. In a second step, their analysis by Flow Field-Flow Fractionation techniques (FIFFF) was examined. They were shown to be very sensitive to shearing, especially during the focus step of the fractionation, and this led to an incompatibility with asymmetrical FIFFF. On the other hand, Frit Inlet FIFFF proved to be very efficient to observe them, either in its symmetrical (FI-FIFFF) or asymmetrical version (FI-AsFIFFF). Conditions of elution were found to optimize the sample recovery in pure water. Spherical self-assemblies were detected, with a size range between 70–400 nm depending on the polymers. Compared to batch DLS, FI-AsFIFFF clearly showed the presence of several populations in some cases. The influence of salt on poly(ethyleneoxide-b-acrylic acid)(PEO-PAA) 6000-3000/dendrigraft poly(L-lysine)(DGL3) was also assessed in parallel in batch DLS and FI-AsFIFFF. Batch DLS revealed a first process of swelling of the self-assembly for low concentrations up to 0.8 M followed by the dissociation. FI-AsFIFFF furthermore indicated a possible ejection of DGL3 from the PIC assembly for concentrations as low as 0.2 M, which could not be observed in batch DLS.

## 1. Introduction

Thanks to the tremendous evolution of polymer engineering over the last thirty years, a large variety of copolymers is now available. This has led to the explosion of polymers able to form different self-assembled nano-objects, using either amphiphilic or double hydrophilic block copolymers. The latter may form associations if one of the blocks is a polyelectrolyte, either weak or strong. In such a case, in the presence of another (block co)polymer of the opposite charge, electrostatic interactions will prevail and expulsion of existing small counter-ions will be favored for entropic rea-

sons, leading to formation of self-assemblies. If the assembly only involves homopolyelectrolytes, it is named interpolyelectrolyte complex (IPEC) [1]. This leads to macroscopic precipitation from the solution for the stoichiometric ratio 1/1 between the cationic and anionic groups. If at least one of the involved polymers is a copolymer exhibiting a neutral block, the assembly is then called “polyion complex micelle” (PICs) or “block ionomer complex” and conditions can be found to maintain its solubility [2–5]. A recent review summarized all the different morphologies described in the literature [1]. Neutral hydrophilic blocks used for PICs include poly(ethyleneglycol), hydrophilic polyacrylates, polyacrylamides, polyoxazolines or poly(vinylpyrrolidone). Polyelectrolyte blocks used have been charged polypeptides, charged polyacrylates or DNAs. Compared to nano-objects formed from amphiphilic block copolymers, PICs exhibit similarities in terms of possible size range (typically from 20 to a few hundred nanometers) and techniques

\* Corresponding authors.

E-mail addresses: frederic.violleau@purpan.fr (F. Violleau), afmingo@chimie.ups-tlse.fr (A.-F. Mingotaud).

for their characterization (classically Dynamic or Static Light Scattering (DLS or SLS) and Transmission Electron Microscopy (TEM)). Marked differences however exist, the strongest one being the sensitivity to salt. Unlike amphiphilic block copolymers assemblies, PICs have been shown to present a very low stability with increasing salt concentration, owing to the displacement of the electrostatic interactions [6,7]. They have been observed, by light scattering, to dissociate for salt concentrations typically higher than 0.5 M. In the case of weak polyelectrolytes, they are also sensitive to pH and the assembly is only observed for a given range of pH [8]. This sensitivity of PICs to both ionic strength and pH has led people to develop stabilization strategies by crosslinking [5,9–12]. PICs are particularly assessed as drug vectors, for instance for photodynamic therapy. The asset of this strategy is that it enables a high encapsulation ratio of the drug, since it is one of the essential blocks of the assembly, acting as a drug vector [10,13–16].

All the nano-objects used for nanomedicine, either formed from amphiphilic or double hydrophilic block copolymers necessitate a characterization that should be as thorough as possible. For this, two techniques are routinely used, namely DLS and TEM. DLS, although routinely used, should be taken with great care [17,18], especially for nano-objects exhibiting a size polydispersity, which is in most cases for polymeric self-assemblies. Furthermore, working directly on a whole solution of nano-objects, DLS can only provide an average value of their size.

On the other hand, TEM enables an individual visualization of the nano-objects, in their dried state. The advantage is then to directly see the objects and their shape, which is not possible with DLS. The drawback however is the limited objects number which is analyzed, since only a part of the solution is imaged. Furthermore, this implies drying of the solution, possibly leading to re-arrangement of the self-assemblies.

In order to improve the characterization of nano-objects, other techniques are also used, such as static light scattering (SLS), neutron (SANS) or X-ray (SAXS) scattering, or cryo-TEM. SANS and SAXS imply correct mathematical fitting of the experimental curves and a difficult accessibility to the instruments [18]. Furthermore, for all batch techniques SLS, SANS or SAXS, the solution being analyzed in its whole, the results are highly dependent on the possible presence of different families of nano-objects. Finally, cryo-TEM enables a direct visualization of the objects without the need for drying them. This powerful method however is sometimes difficult to perform in order to obtain clear glassy ice, and a large dispersity in size of the nano-objects may be complex to analyze owing to different positioning of the nano-objects on the grid during the fast freezing process (linked to the thickness of the ice layer, that might be close to the size of the nano-objects themselves).

This quick overview of the analysis techniques for nano-objects points out the great difficulty to have a thorough characterization, especially because of the polydispersity of the samples. In order to use these techniques while limiting the influence of polydispersity, their combination with fractionation techniques is a choice approach. Indeed, regular chromatography such as Size Exclusion Chromatography should be avoided for self-assemblies, since the presence of the stationary phase together with high shearing during elution might lead to modification of the assemblies. For this reason, Field-Flow Fractionation (FFF) techniques and mainly Flow FFF have been increasingly assessed as separation methods for nanoparticles and are associated to subsequent characterization by RI, multi-angle light scattering (MALS), UV-vis or DLS detection [19]. In a recent review, Roda et al. explained that the application of current nanotechnologies suffered from the present difficulty of developing well defined nanoparticles, or efficient techniques to characterize the existing ones. FFF was developed more than 30 years ago and the technical progresses have enabled its use in various domains such as environmental, food, polymer and phar-

maceutical industry analyses [20–29]. Samples injected into FFFF systems require a separate relaxation process prior to the separation. This process is essential to FFF as sample components are ‘relaxed’ into different equilibrium positions and thus different velocity streamlines of the parabolic flow profile. For a conventional symmetrical Flow FFF channel, the axial flow is stopped for a certain period to allow this relaxation process to take place. For an Asymmetrical Flow FFF, sample relaxation is normally achieved by using a focusing process. While the stop-flow and focusing processes are essential in each flow FFF sub-technique, they may lead to baseline fluctuations and to undesirable particle interactions with the channel wall [30,31].

The unwanted effects of stop-flow and focusing processes can be avoided by using hydrodynamic relaxation methods that were introduced by implementing a split inlet or a frit inlet [31,32] in a symmetrical flow FFF channel. In the same way, Moon and colleagues described extensively [33–39] a frit inlet injection technique applied to an asymmetrical flow FFF channel to allow a stop-less sample injection. With the application of a hydrodynamic relaxation technique using a frit inlet in asymmetrical flow FFF, the focusing process can be completely avoided. This technique has shown its efficiency for fractionation of different macromolecules and particles like lipoprotein particles [40], carbon nanotubes [41], sodium hyaluronate [42–44] and ultrahigh-molecular weight cationic polyacrylamide [45] reducing risk of adsorption on the FFF membrane and/or sample aggregation.

In this work, we demonstrate that Asymmetrical Flow Field-Flow Fractionation (AsFIFFF) is a powerful method to characterize polymeric micelles and vesicles [46–49], explicitly showing the relative ratio of different populations of self-assemblies in a sample, where batch DLS only showed the largest populations. In order to further diversify the application domain of FFF, we assessed the characterization of different PICs, based either on commercial or home-made polymers. Indeed, to the best of our knowledge, only a few studies have described the use of FFF techniques for the characterization of charged polymers assemblies. Two of them studied polyelectrolyte complexes using As-FIFFF [50,51] involving two oppositely charged homopolymers. Another described As-FIFFF analysis of poly(ethylene oxide-*b*-sodium methacrylate)/poly(methacryloxyethyl trimethylammonium chloride) self-assemblies which are the most similar to the PICs of our work [52]. This unique literature example on PICs characterization by FFF showed that further studies are needed in order to assess the usefulness of FFF techniques for such self-assemblies.

## 2. Materials and methods

### 2.1. Chemicals

Poly(acrylic acid) (PAA) and Poly(lysine) PLys (15000–3000 g mol<sup>-1</sup>) were purchased from Aldrich, poly(ethyleneoxide-*b*-acrylic acid) (PEO-PAA) from Polymer Source Inc. (Dorval Montréal, Canada), dendrigraft polylysine (DGL) from Colcom (Montpellier, France). Poly[(3-acrylamidopropyl) trimethylammonium chloride - *b* - *N* - isopropyl acrylamide] (PAPTAC-PNIPAM) was kindly provided by M. Destarac (IMRCP laboratory) and was synthesized by RAFT polymerization [53].

### 2.2. Formation of PICs

PEO-PAA/DGL3 PICs were prepared by mixing DGL3 (5 mg mL<sup>-1</sup>) stock solution at pH 7 with adequate amounts of PEO-PAA (1 mg mL<sup>-1</sup>) stock solution at pH 7 in order to have the same concentration of carboxylic acids and amino groups. These solutions

were further diluted with water in order to achieve a final DGL3 concentration of 0.1 wt%.

In a similar way, PEO-PAA/PLys solutions were obtained by addition of 85  $\mu\text{L}$  of PEO-PAA 5–38 in phosphate buffer pH 7.4 ( $2\text{ mg mL}^{-1}$ ) to 3 mL LysHBr in phosphate buffer pH7.4 ( $0.16\text{ mg mL}^{-1}$ ).

PAPTAC-PNIPAM and PAA (adjusted pH at 5.5 by adding NaOH solution) were separately dissolved in water, giving clear colorless solutions. PAPTAC-PNiPAM/PAA PICs were prepared by mixing appropriate amounts of each polymer, at a desired stoichiometric ratio, and water to obtain the right concentration. First a volume of PAPTAC-PNIPAM solution and water were mixed, and then the appropriate amount of PAA solution was added.

PEO-PAA/DGL3 PICs at different NaCl concentrations were obtained by mixing, in the following order, DGL3 mother solution (0.5 wt%) at pH 6.7, water, PEO-PAA stock solution (0.5 wt%) at pH 7 and NaCl stock solution (6 M). PEO-PAA stock solution was added in order to have a ratio of 1 between carboxylic acid and amino groups. Adequate amounts of NaCl stock solution were added in order to have a final salt concentration of 0.2, 0.8, 1 and 2 M. Pure water was added in order to get a final DGL3 concentration of 0.1 wt%.

### 2.3. Dialysis follow-up

Solutions of PEO-PAA 6-3/DGL3 PIC in 0.2 and 2.0 M NaCl solutions were formed by mixing varying volumes of polymer solutions in water to concentrated 4 M NaCl solution. 3 mL of these solutions were introduced in dialysis flasks (GE Healthcare Bio-Sciences membranes with a MWCO of  $1000\text{ g mol}^{-1}$ ) and dialyzed against 800 mL of milli-Q water. The dialysis process was interrupted at specific times in order to perform DLS analysis.

### 2.4. DLS

DLS was carried out at  $25^\circ\text{C}$  on a Malvern Zetasizer NanoZS equipped with a He-Ne laser ( $\lambda=633\text{ nm}$ ). Solutions were analyzed as synthesized without filtration to ensure that large populations were not discarded from analysis. Polydispersity indices (PDI) were obtained from the correlation function by using a cumulant analysis. The correlation function was analyzed *via* the general-purpose non-negative least squares (NNLS) method to obtain the intensity-weighted distribution of diffusion coefficients (D) of the solutes. This distribution can be converted, using Mie theory, to a number-weighted distribution describing the relative proportion of multiple components in the sample based on their number rather than based on their scattering. The average apparent hydrodynamic diameters, noted as 'DLS Size<sub>int</sub>' or 'DLS Size<sub>Number</sub>', were determined using the Stokes-Einstein equation from intensity-weighted and number-weighted distributions, respectively. Unless stated, the term size refers to diameters. Each solution was analyzed 3–5 times depending on the observed correlogram. The typical accuracy for these measurements was 10–20% for systems exhibiting a polydispersity index (PDI) lower than 0.4. This PDI is defined as the ratio between the second moment of the distribution divided by the square of the mean value of the decay rate. The values presented in the tables are not mean values, because this is not relevant for DLS analysis of multi-population samples. Indeed, in such case, the DLS software will exhibit a larger inaccuracy for the least present population. Thus, the results presented in the tables are those obtained for a typical result for each analysis.

The Malvern DLS data were further analyzed by a custom-made program named STORMS in order to obtain a more precise characterization of the solutions. This program has been designed with Matlab<sup>®</sup> and enables the fitting of DLS correlograms using different sets of parameters, corresponding to all hypotheses that have to be made for fitting the correlograms. Indeed, going from correlograms

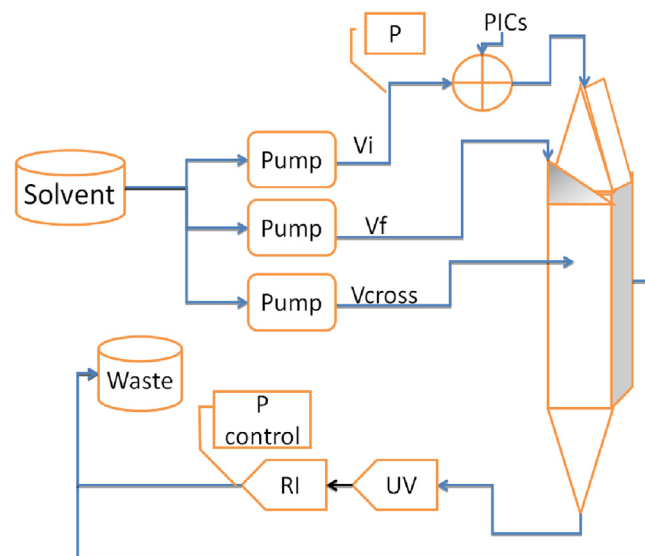
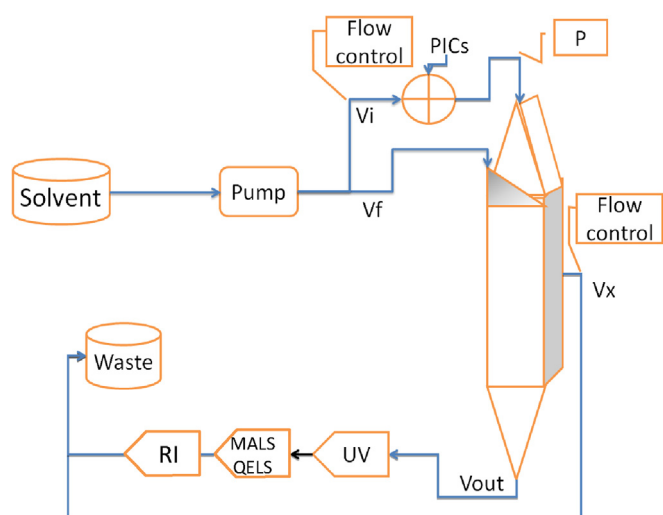


Fig. 1. Experimental set-up for Symmetrical FFF.

to size results implies three levels of hypotheses: the first consists of the transformation of autocorrelation data to diffusion coefficient, the second extracts the size of the scattering object from diffusion coefficient depending on its geometry, and finally uses a model enabling the transformation of the intensity-relative population to a number-relative equivalent. For each step, STORMS provided the choice of different parameters. For the nano-objects presented here, the protocol used a non negative least squares (NNLS) fitting, assumed a spherical shape for all objects, and the chosen scattering model was that corresponding to spheres (Rayleigh or Mie's model depending on the size). The range of decay rates and the regularization parameter were systematically modified to check the consistency of the results (supplementary information). Unless stated, this treatment provided residuals lower than  $5 \times 10^{-3}$  for all analyses. The estimated PDI in STORMS is often larger than that calculated by the MALVERN software since all the experimental points are selected and the second order equation is used in STORMS instead of the third one for Malvern.

### 2.5. Frit inlet symmetrical FIFFF (FI-FIFFF)

A Frit-inlet Frit-outlet Symmetrical Flow Field-Flow Fractionation channel (FFFractionation, Salt Lake City, UT) was used and eluent was supplied by three pumps (Waters 510 HPLC and two Waters 590 HPLC) as depicted in Fig. 1. The accumulation wall was a 1 kDa cut-off regenerated cellulose ultrafiltration membrane (Postnova Analytics, Landsberg am Lech, Germany). The sample injection was triggered manually with a 6-way valve into the Frit-inlet SyFIFFF channel. A pressure controller (custom made) was installed after the detectors. The eluting sample components were detected with a Water 410 Refractometer (Waters US) and a UV detector (Waters 486 Tunable Absorbance Detector (401 nm)). An aqueous 0.02 wt% sodium azide solution was filtered (vacuum filtration system with 0.1  $\mu\text{m}$  pore size Gelman filters) before use as eluent. The spacer type was 250S which corresponded to  $\sim 250\text{ }\mu\text{m}$  thickness. Samples were injected at a 0.5 wt% concentration. The elution program used for the cross flow rate  $V_{\text{cross}}$  was  $0.6\text{ mL min}^{-1}$  during all the tests while  $V_i$  and  $V_f$  were subjected to variation from 0.4 to 1.2 and from 0 to  $8\text{ mL min}^{-1}$ , respectively.



**Fig. 2.** Experimental set-up for Asymmetrical FFF.

### 2.6. Frit Inlet Asymmetrical Flow Field-Flow Fractionation (FI-AsFFFF)

A Frit-inlet Asymmetrical Flow Field-Flow Fractionation channel was linked to an Eclipse 3 system (Wyatt Technology Europe, Dernbach, Germany, Fig. 2). The accumulation wall was a 1 kDa cut-off regenerated cellulose ultrafiltration membrane (ConSensuS, Ober-Hilbersheim, Germany). An Agilent 1100 Series Isocratic Pump (Agilent Technologies, Waldbronn, Germany) with an in-line vacuum degasser and an Agilent 1100 Autosampler delivered the carrier flow and handled sample injection into the Frit inlet AsFFFF channel. A 0.1 mm in-line filter (VVLP, Millipore, Germany) was installed between the pump and the FFF channel. An aqueous 0.02% sodium azide solution was filtered (vacuum filtration system using 0.1 mm Gelman filters) before use as eluent. The spacer type was 250S or 350S (250  $\mu\text{m}$  or 350  $\mu\text{m}$ , respectively). Samples were injected either at a 0.5 or 0.1 wt% concentration. The elution program used for injection flow  $V_i$  of 0.2 mL  $\text{min}^{-1}$  and for detector flow  $V_{\text{out}}$  of 1 mL  $\text{min}^{-1}$  for cross flow  $V_x$  was 0.5 mL  $\text{min}^{-1}$  for 2 min, 2 mL  $\text{min}^{-1}$  for 38 min, decreased to 0.5 mL  $\text{min}^{-1}$  in 10 min followed by 0.5 mL  $\text{min}^{-1}$  for 40 min. The eluted sample components were detected with Multi-Angle Light Scattering (MALS) DAWN Heleos II (Wyatt Technology, Santa Barbara, CA, US) equipped with a DLS (DLS) at 99° and an OptilabRex Refractometer (Wyatt Technology, Santa Barbara, CA, US) detectors. The MALS detector was normalized with bovine serum albumin (BSA). Calibration of scattering intensity was performed with HPLC-grade filtered toluene.

## 3. Results and discussion

### 3.1. Formation of PICs

Different polymers were used to form the self-assemblies (Fig. 3 and Table 1), having acidic (PEO-PAA and PAA) or amino or ammonium groups (PLys, DGL, PAPTAC-PNIPAM). DGL is a dendrigraft form of polylysine. These polymers were chosen in order to have a variety of molar masses and architectures. PICs were formed by direct mixing of two solutions of the constituents at appropriate pH. The studied pairs were PEO-PAA/DGL, PEO-PAA/PLys and PAPTAC-PNIPAM/PAA.

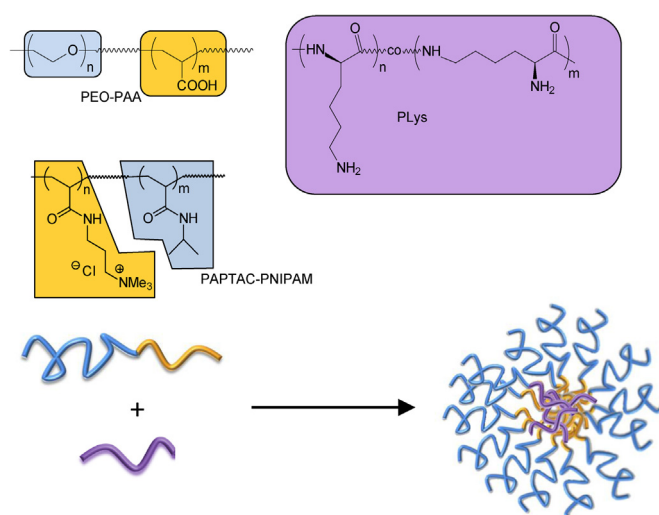


**Fig. 3.** Polymers used for PICs formation.

**Table 1**

Molar masses of the polymer used as controlled by SEC and  $^1\text{H}$  NMR (Table S1 in Supplementary material).

Name	Mn block 1 ( $\text{g mol}^{-1}$ )	Mn block 2 ( $\text{g mol}^{-1}$ )
PEO-PAA 5-38	5000	38000
PEO-PAA 6-3	6000	3000
PEO-PAA 6-6.5	6000	6500
PEO-PAA 6-12	6000	12000
PEO-PAA 11-4	11000	4000
PEO-PAA 28.6-21.1	28600	21100
PLys	70000	
DGL3	18700	
PAA 10	10000	
PAA 1	1000	
PAPTAC-PNIPAM 1-9	1000	9000
PAPTAC-PNIPAM 16.9-3.1	16900	3100

### 3.2. DLS characterization

The formation of assemblies was first confirmed by classical batch DLS (Fig. 4 and Table 2), using data obtained from Malvern instrument followed by fittings by a custom-made software, STORMS, enabling extensive parameter fitting. This software is further described in supplementary information, together with a discussion comparing Malvern to STORMS results. Nano-objects exhibited a size range between  $\sim 10$  and 250 nm, ensuring a diversity of objects.

Some of the self-assemblies presented a bimodal population in the intensity relative results as shown in Fig. 4, but results in number relative average were all monomodal (Figs. S2–S6 in Supplementary material). All polydispersities were in the range 0.1–0.4, indicative of reasonably well defined systems. It is noteworthy that, generally speaking, the estimated PDI in STORMS is larger than the one calculated by the MALVERN software since all the experimental points are selected and the second order equation is used in STORMS instead of the third order for Malvern (see supplementary information). The observed sizes are not linked to the molar masses of the copolymers, but a trend shows that low fractions of the polyelectrolyte block (defined as  $M_{\text{polyelectrolyteblock}}/M_{\text{copolymer}}$ ) tend to lead to small PICs, whereas high fractions may yield large objects (Fig. S7 in Supplementary material).

**Table 2**  
DLS diameters of PICs.

PIC	DLS size <sub>int</sub> (nm)	PDI <sup>a</sup> <sub>int</sub>	DLS size <sub>number</sub> (nm)	PDI <sup>a</sup> <sub>number</sub>
PAPTAC-PNIPAM 1-9/PAA 10	75	0.2	58	0.2
PAPTAC-PNIPAM 16.9-3.1/PAA10	222	0.1	210	0.07
PAPTAC-PNIPAM 16.9-3.1/PAA 1	252	0.21	204	0.05
PEO-PAA 6-3/DGL3	42 <sup>b</sup>	0.39	32	0.19
PEO-PAA 6-6.5/DGL3	58	0.28	42	0.21
PEO-PAA 6-12/DGL3	92	0.15	86	0.1
PEO-PAA 11-4/DGL3	67	0.29	45	0.23
PEO-PAA 28.6-21.1/DGL3	50 <sup>b</sup>	0.33	36	0.21
PEO-PAA 5-38/DGL3	166	0.2	132	0.18
PEO-PAA 5-38/PLys	90 <sup>b</sup>	0.3	44	0.3

<sup>a</sup> polydispersity indices.

<sup>b</sup> bimodal distribution.

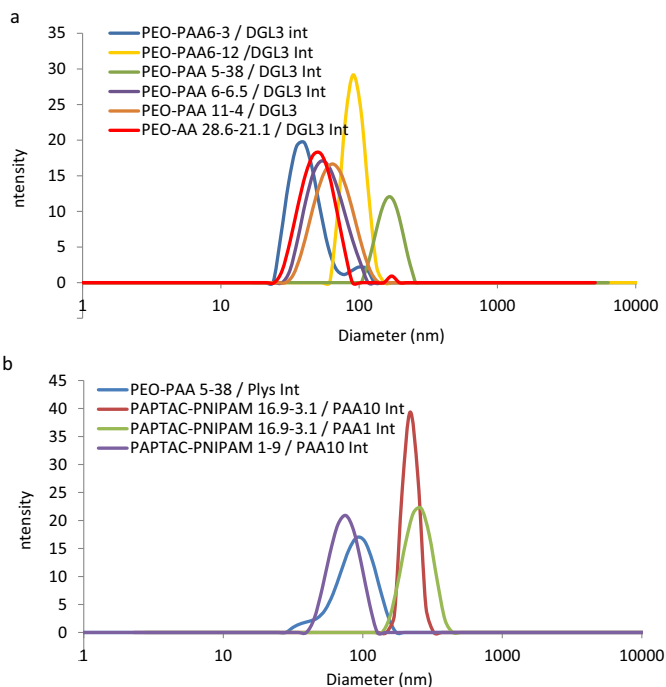


**Fig. 4.** DLS analysis of the different PICs, intensity relative analysis. a: PEO-PAA/DGL3 PICs; b: other PICs.

### 3.3. Frit-Inlet FIFFF

Based on our experience with polymeric self-assemblies [47,49], some of the formed PICs were first evaluated by AsFIFFF. The obtained fractograms were observed to be erratic (data not shown), in some cases even leading to the absence of peaks after elution. Recovery tests (see supplementary information pS12) showed PICs sensitivity during the essential focus step. The amount of detectable product rapidly decreased during the focus step, even for low flow rates. This phenomenon led us to test the performance of Frit Inlet techniques, to eliminate the stop-flow (FIFFF) and focusing step (AsFIFFF), suspected to be the cause of the PICS degradation observed in conventional AsFIFFF channel.

Recovery tests were first performed using Frit-Inlet Symmetrical Flow FFF for a typical PIC, namely stoichiometric PAPTAC-PNIPAM 1-9/PAA10. The RI peak area was recorded for different elution conditions (Fig. 5). The maximum theoretical area was obtained in the absence of channel and was used as a reference. Adding the channel alone led to a 20% decrease of the PIC peak area. The addition of crossflow  $V_{cross}$  did not lead to a further decrease, and a cross-flow at  $0.6 \text{ mL min}^{-1}$  was therefore chosen for all experiments. The injection flow rate was also observed to have no influence on the

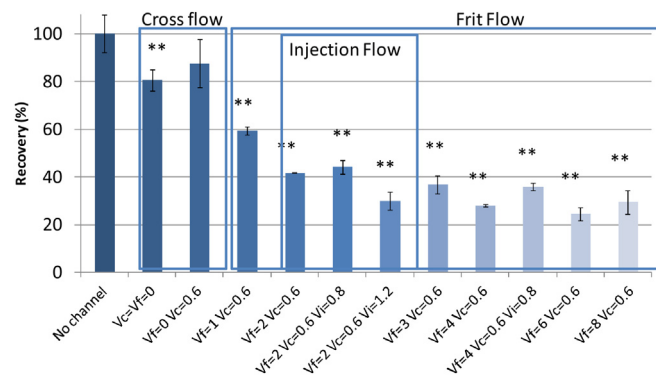


**Fig. 5.** Recovery tests for PAPTAC-PNIPAM 1-9/PAA10. Unless noted, all injections were performed using an injection flow rate  $V_i = 0.4 \text{ mL min}^{-1}$ . Dunnett's test: \* =  $p < 0.05$  \*\* =  $p < 0.01$ .

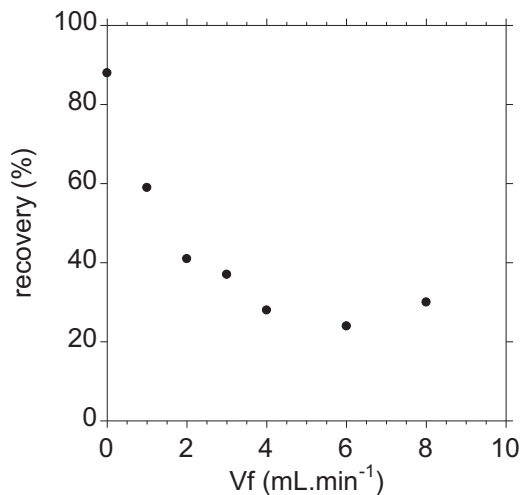


**Fig. 6.** Recovery of PAPTAC-PNIPAM 1-9/PAA10 by FI-FIFFF,  $V_i = 0.4 \text{ mL min}^{-1}$ ,  $V_{cross} = 0.3 \text{ mL min}^{-1}$ .

sample recovery. An injection flow rate at  $0.4 \text{ mL min}^{-1}$  was therefore chosen. Finally, the flow rate  $V_f$  used in the Frit inlet device was observed to have a strong influence on the recovery of the objects (Fig. 6). The recovery decreased to ~30% for  $V_f = 4 \text{ mL min}^{-1}$ . A higher  $V_f$  did not affect the recovery;  $V_f$  was thus fixed at  $4 \text{ mL min}^{-1}$ .

In conventional symmetrical FIFFF (SyFIFFF) analyses, a stop flow step is present prior to fractionation where the channel flow is turned off and only the cross flow field is applied to the sample for several minutes [54]. This step allows for analyte relaxation to a steady state equilibrium height near the accumulation wall with

smaller analytes positioned higher in the channel on average than larger analytes (in the normal mode of FFF). However, it is important to note that the highest sample concentration exists at the semi-permeable membrane accumulation wall [55]. High sample concentrations have been shown to cause sample loss due to irreversible sample adsorption to the membrane [56,57]. Additionally, if components of the PICs are smaller than the molecular weight cut-off of the semi-permeable membrane they can pass through the membrane resulting in lower sample recovery [58]. The use of a frit-inlet flow near the beginning of the channel in addition to constant channel and cross flows eliminates the need for the stop-flow relaxation procedure [31]. This frit-inlet flow rapidly forces analytes towards the accumulation wall allowing for sample relaxation under continuous channel and cross flow conditions. Frit-inlet SyFIFFF (FI-SyFIFFF) can reduce sample loss due to membrane interactions or filtration by avoiding the stop-flow step [59,60]. The absence of stop-flow during Frit-inlet FIFFF resulted in improved sample recovery for PICs and demonstrated the performance of this

method for the PICs analysis. However, the improved sample recoveries are still relatively low (20–60%). As described by Wahlund, the use of Frit-inlet (FI-AsFIFFF) should increase the performance of this analysis, by improving resolution and giving less sample dilution [61].

PIC PAPTAC-PNIPAM 1-9/PAA10 was also analyzed by FI-AsFIFFF. As presented in Table 3, optimization of  $V_f$  showed that it was possible to obtain higher recoveries in FI-AsFIFFF (up to 77%) compared to FI-SyFIFFF (<60%). Moreover, this system gives the opportunity to development methods using a  $V_{cross}$  gradient. Typical recoveries obtained for the different PICs assemblies are reported in Table 3, showing that for most systems, very good recoveries were obtained, ensuring trustful analyses of the self-assemblies.

Fractograms (signal RI and MALS) of PICs for stoichiometric ratios between acidic and basic moieties are presented in Fig. 7(A–G). For PICs with PEO-PAA 6-3 and 6-12 (Fig. 7B and D), a residual peak of DGL at 6.5 min could be observed and the PIC

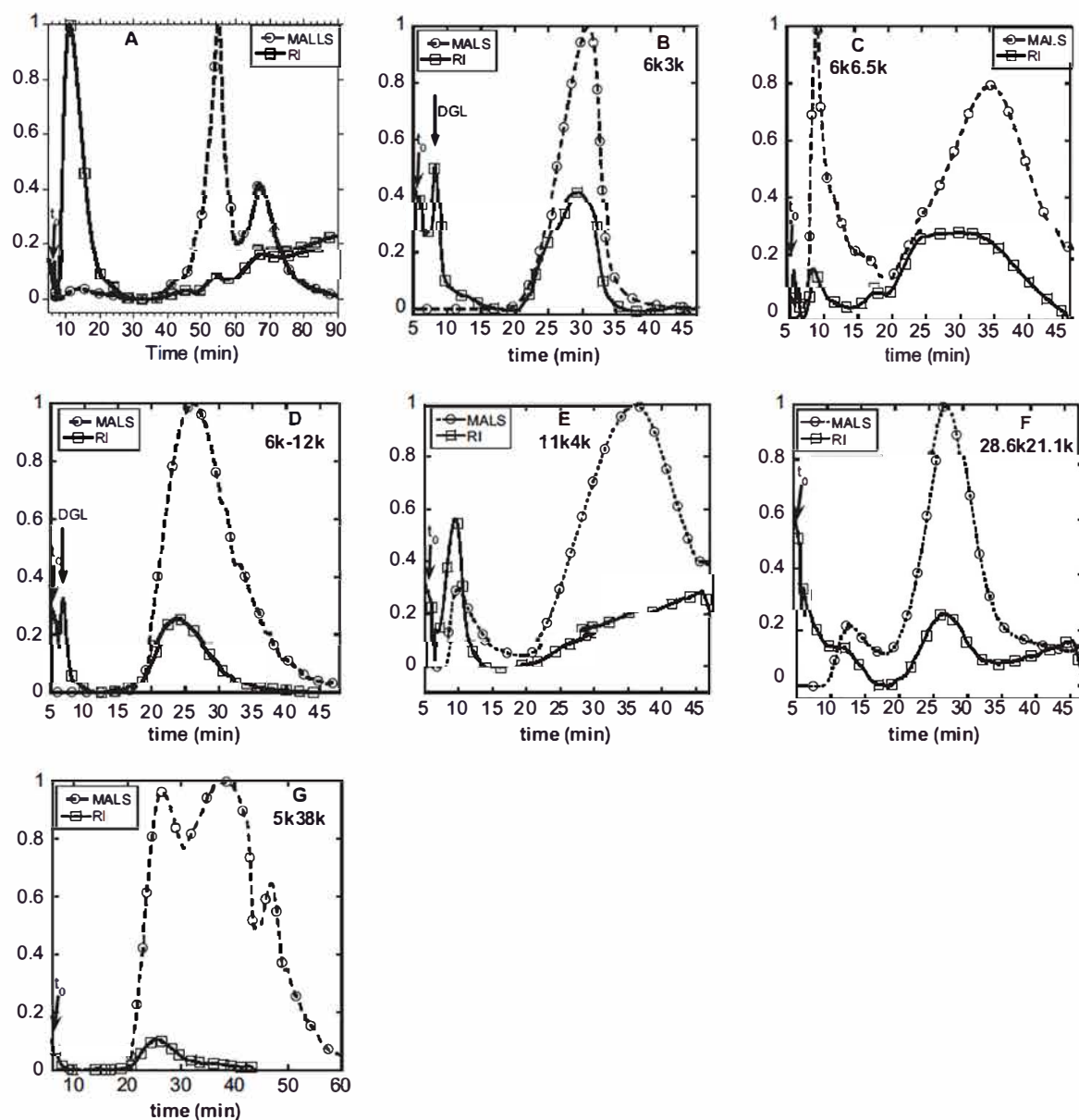


Fig. 7. Frit-Inlet FFF fractograms for PAPTAC-PNIPAM 1-9/PAA 10 (A) and PEO-PAA/DGL3 PICs. The letter corresponds to the line in Table 3.  $V_{out}$  1 mL.min<sup>-1</sup>,  $V_x$  2-0.5 mL.min<sup>-1</sup>,  $V_i$  0.2 mL.min<sup>-1</sup>. PICs with PEO-PAA 6-12 and 5-38 were eluted with a spacer of 350S, whereas all others were characterized with a 250S spacer.

**Table 3**  
FI-AsFIFFF analysis of different PICs ( $V_{out}$  1 mL min<sup>-1</sup>,  $V_x$  2–0.5 mL min<sup>-1</sup>,  $V_i$  0.2 mL min<sup>-1</sup>).

	Polymer 1	Polymer 2	Recovery (%)	Peak 1				Peak 2			
				elution time (min)	$R_h$ (nm) (n) <sup>a</sup>	$R_g$ (nm) (nm) <sup>ab</sup>	$R_g/R_h$ <sup>b</sup>	elution time (min)	$R_h$ (nm) (nm) <sup>a</sup>	$R_g$ (nm) (nm) <sup>ab</sup>	$R_g/R_h$ <sup>b</sup>
A	PAPTAC-PNIPAM 1-9	PAA 10	77	14	50 <sup>b</sup>	<10 <sup>c</sup>	–	54/66	100/200	30/40	0.3/0.2
B	DGL3	PEO-PAA 6-3	99	30	27	17	0.62				
C	DGL3	PEO-PAA 6-6.5	100	10	148	64	0.43	35	69	36	0.52
D	DGL3	PEO-PAA 6-12	97	25	35	25	0.71				
E	DGL3	PEO-PAA 11-4	40	9	107	32	0.30	35	35	21	0.6
F	DGL3	PEO-PAA 28.6-21.1	80	12	193	65	0.34	28	98	25	0.26
G	DGL3	PEO-PAA 5-38	71	25	38	26	0.68	38	53	46	0.87

<sup>a</sup> number averaged values. For comparison, Table S5 presents the other average types.

<sup>b</sup> The used  $dn/dc$  (measured or estimated) are presented in supplementary information (Table S4).

<sup>c</sup> inaccuracy > 20%, not trustful value.

formation was evidenced by the presence of a major peak eluting around 20–35 min. For all other systems (Fig. 7A, C, E–G), the PICs were observed as bimodal populations. The corresponding  $R_h$  obtained from DLS and  $R_g$  are also reported in Table 3. If the recovery of all systems was high, the results of the obtained sizes are somewhat surprising. For this size range of nano-objects, normal mode elution is expected and small objects should elute faster than larger ones. Here, it is very surprising that nano-objects of  $R_h \sim 100$ –200 nm were observed for elution times as small as 9–10 min, whereas 30–100 nm PICs eluted after 25 min. It is possible that the large analytes eluting at 9–10 min have stronger repulsive interactions with the membrane than the PICs eluting at later times. This earlier than expected elution is possible if the chemical compositions of the two populations are different. Indeed, high adsorption of PEO-PAA copolymers with FFF channel membrane in a salt-free eluent did not permit the analysis of the copolymers (data not shown). It is noteworthy that in the only other published As-FIFFF characterization of a PIC, elution involving both normal and steric processes was observed [52]. In our case, such a dual process could also be considered.

FI-AsFIFFF hyphenated with online MALS and DLS also gave access to the  $R_g/R_h$  ratio, indicating the morphology of the nano-object. PICs in the literature have been observed to exhibit  $R_g/R_h$  ratios over a very wide range, from 0.3 to 1.3, depending on the more or less defined core-shell morphology and the density of the core [3,7,8,62–67]. The values found in this work suggest objects with a dense core for those close to 0.3–0.4 or homogeneous spherical ones for  $R_g/R_h$  close to 0.7–0.8 [18,68]. Further characterization of the shape and internal structure of the objects, in particular by SAXS, is under way.

Although molecular weights are provided by the program, we decided not to give them, since their determination is based on identified refractive index increments. In the cases presented here, all fractograms exhibited either a residual DGL peak or several PICs peaks indicative of mixtures. In such conditions, the actual composition of each peak cannot be determined.

Comparing the results obtained by FFF and batch DLS shows different cases. For PICs based on PEO-PAA 6-3 and 11-4 and those of PAPTAC-PNIPAM 1-9/PAA10, the results are in good agreement for both methods. PICs based on PEO-PAA 6-6.5 and 28.6-21.1 exhibited a much larger size in FFF compared to batch DLS. Finally, those based on PEO-PAA 6-12 and 5-38 presented smaller sizes by FFF compared to batch DLS. At this point, no clear explanation can be provided, although differences in interactions with the FFF membrane could have an influence.

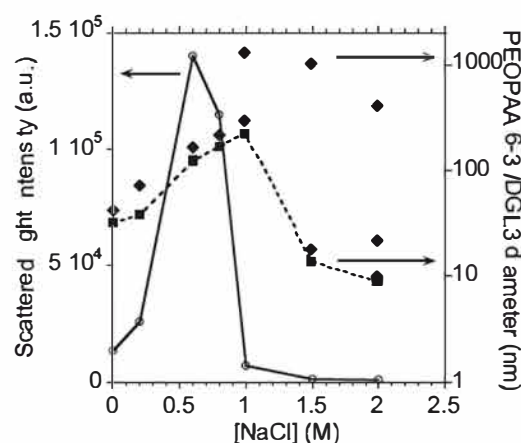


**Fig. 8.** Influence of NaCl concentration on DLS batch analysis for PEO-PAA 6-3/DGL3. o: scattered light intensity;  $\blacklozenge$ : intensity relative diameter;  $\blacksquare$ : number relative diameter.

### 3.4. Additional studies of PICs stability in the presence of salt

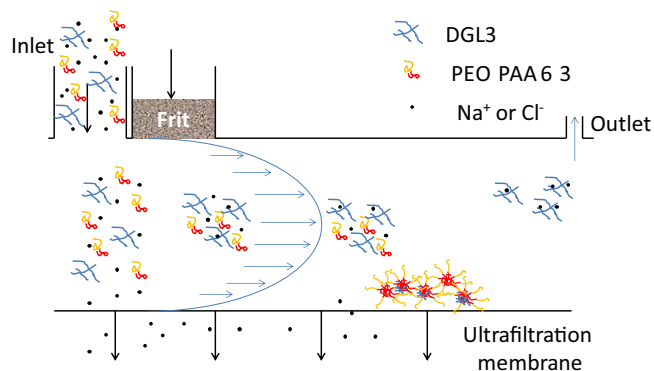
PEO-PAA/DGL3 PICs were further characterized in the presence of increasing NaCl concentration. The solutions were analyzed both by batch DLS and FI-AsFIFFF. The results of batch DLS are presented in Table 4 and Fig. 8. Upon addition of NaCl, the scattered light intensity increased for concentrations up to 0.6 M and subsequently severely decreased to near-zero values for concentrations higher than 1.5 M. The intensity and number relative sizes increased for low concentrations of salt, a sign of swelling of the self-assembly, followed by their complete dissociation. Above 1 M, fitting of the correlograms indicated the presence of several populations of nano-objects, rendering the interpretation difficult (Fig. S9 in Supplementary material). The comparison between intensity and number relative diameters showed that very large uncontrolled aggregates were formed in small quantities. This behavior shows that addition of salt severely destabilized the self-assembly, which has been already described in the literature [6,7].

FI-AsFIFFF was used to obtain more information. In order to limit the drawback of FFF analysis in high salt concentration conditions with  $V_x$  gradient (drift of RI signal), we decided that all FFF elutions be carried out in pure water. The PICs were prepared in pure water, then exposed to increasingly high concentrations of salt and then eluted by FFF in pure water. Therefore, a difference existed between the analyses by FI-AsFIFFF (samples in NaCl solutions, but eluted in pure water) and those by batch DLS (samples in NaCl solutions, analyzed directly). This also implied that during elution, a

**Table 4**

Batch DLS characterization of PEO-PAA 6-3/DGL3 with increasing concentrations of NaCl.

[NaCl]	DLS size <sub>int</sub> (nm)	% int	PDI <sub>int</sub>	DLS size <sub>number</sub> (nm)	PDI <sub>number</sub>	Scattered light intensity (a.u.)
0	42		0.39	32	0.19	13 500
0.2	72	99	0.60	38	0.20	25 800
0.6	166		0.23	124	0.20	140 000
0.8	216		0.20	168	0.18	114 800
1.0	1320 <sup>a</sup>	74	2.5	228	0.48	7 000
	300	12				
1.5	1040	85	7.20	14	0.17	1 300
	18	13				
2.0	410	58	1.2	9	0.15	1 000
	22	17				
	10	13				

<sup>a</sup> presence of very large aggregates (>1  $\mu\text{m}$ ).**Fig. 9.** Frit Inlet FFF elution of PEO-PAA 6-3/DGL3 solutions, in the case of high NaCl concentration.

desalting process took place. This has to be taken into account for the discussion, especially for the highly concentrated solutions for which the sample mainly consisted in soluble polymers whereas desalting might lead to re-assembly during elution (Fig. 9). In order to assess the rate of re-assembly by desalting, a control experiment was performed, where NaCl solutions of PEO-PAA 6-3/DGL3 PICs were submitted to dialysis and batch DLS was performed at different times. The results (Figs. S10 and S11 in Supplementary material) showed that for low concentrations of salt (0.2 M), the PIC self-assembly remained stable. For the high 2 M concentration, desalting led to the formation of uncontrolled self-assembly between 15 and 60 min. This means that samples analyzed by FI-AsFIFFF were subjected to the influence of salt in the initial solution and possibly to the desalting process.

The different fractograms are reported in Fig. 10. Increasing the concentration of salt led to three concomitant processes: increase of the DGL peak at 6.8 min, displacement of the PIC peak for high concentrations of NaCl and increase of the light scattering signals after 50 min of elution. The increase of DGL peak at 6.8 min is attributed to an ejection of DGL from PIC in the presence of salt. This process was observed for NaCl concentration of 0.2 M, where desalting effect had no influence on the PIC stability. This process can therefore be assumed to occur for all NaCl concentrations, even in the presence of desalting during elution. Also, from the high intensity of the peak compared to pure DGL, it can be assumed that chloride ions were also associated with DGL. If DGL is ejected from PIC self-assembly, the resulting nano-objects that were analyzed presented therefore a drift in composition from the ideal 1/1 acid/amine ratio. Therefore, the radius of gyration of molecular weight of the self-assemblies cannot be determined accurately.

The aggregates that were observed after 50 min were released owing to a decrease in the crossflow. Interestingly, although instantaneous DLS correlograms were difficult to interpret, a mean hydrodynamic diameter of 400 nm was obtained (Table 5), which

**Table 5**

FI-AsFIFFF analysis of PEO-PAA 6-3/DGL3 PIC in the presence of NaCl.

[NaCl]	Peak 1		Peak 2	
	elution time (min)	$R_h$ (n) (nm) <sup>a</sup>	elution time (min)	$R_h$ (n) (nm) <sup>a</sup>
0	28	27		
0.2	28	27	56	100
0.8	23	40	58	80
1.0	24	"200"	>50	"200"
2.0	24	"200"	>50	"200"

<sup>a</sup> number averaged values.

is close to the size observed by batch DLS in the intensity relative analysis.

The remaining peaks between 20 and 35 min were observed to exhibit a size between 50 and 80 nm for salt concentrations lower than 0.8 M, whereas their size was found close to 400 nm for higher concentrations. It should be noted that analytes with sizes of  $\sim 400$  nm could be near the steric transition point where elution switches from normal to steric mode. However, one has to take also into account that, for 2.0 M salt solutions, the desalting process has been shown to lead to re-assembly between 15 and 60 min, which corresponds to the elution time in FI-AsFIFFF. One can therefore not reject the possibility that the peaks observed at 25 min in this case were in fact self-assemblies produced in the channel during elution.

In the study carried out by Wiedmer [52] on poly(ethylene oxide-*b*-sodium methacrylate)/poly(methacryloxyethyl trimethylammonium chloride), the resistance of the PIC assembly towards NaCl was also considered, however at low concentrations between 0.02 and 0.16 M. Swelling was observed, in concordance with our work. Cases of bimodal distributions were also observed. In their case, As-FIFFF thus led to good characterization. However, it is noteworthy that the molar mass of their cationic polymer was close to  $300,000 \text{ g mol}^{-1}$ , which is much higher than the polymers used here. It is therefore possible that this higher molar mass gives a better resistance to focus by the presence of longer chains that can act as anchor in the case of shearing.

#### 4. Conclusion

Polyion complex self-assemblies based on different polymers or copolymers have been formed and analyzed in this work. Batch DLS and FFF characterizations have been cross-examined and have confirmed the strength of FFF when several populations are present. However, it is noteworthy that Frit-Inlet FIFFF was necessary in our case for correct analysis of the PICs, owing to dissociation of the self-assemblies upon focusing with regular AsFIFFF. FI-AsFIFFF also enabled us to characterize the evolution of the self-assemblies in the presence of NaCl and showed a possible ejection of one of the component from the PIC, leading to a drift in the composition

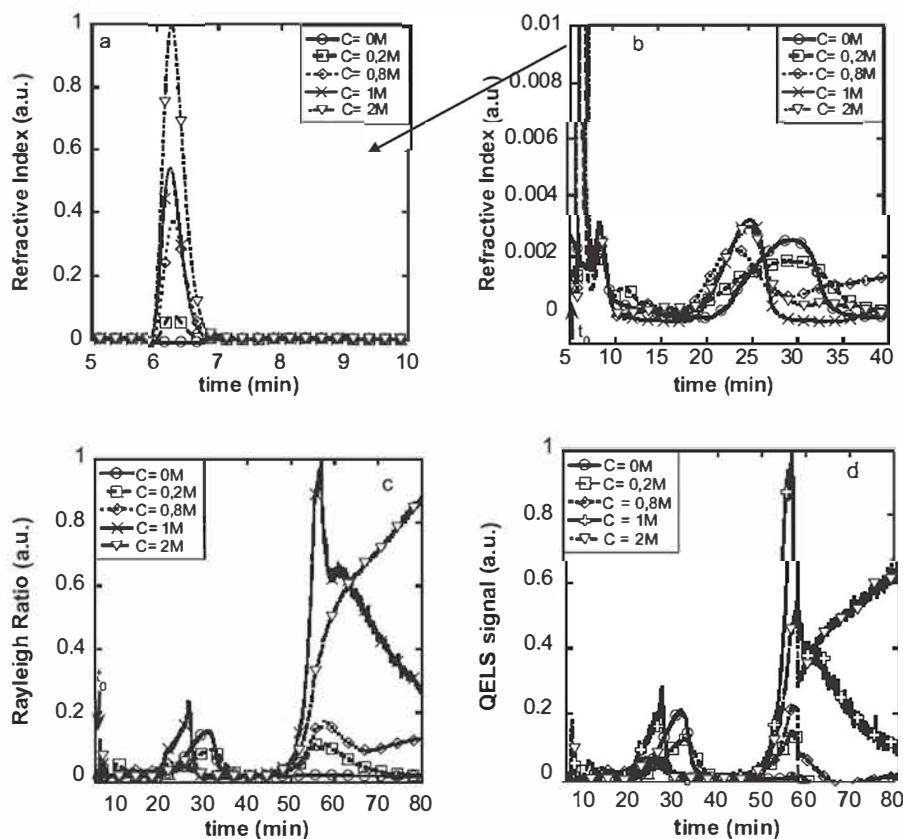


Fig. 10. FI-AsFFFF of PEO-PAA 6-3/DGL3. a and b: refractive index signal; c: MALS signal; d: DLS signal.

of the PIC's peak in the fractograms. PICs systems are known to be very complex assemblies, owing to their possible dissociation. Their thorough characterization therefore implies the use of multiple techniques to better understand their behavior. Ongoing studies are currently performed in our teams for this, but this work has clearly established FFF as a powerful technique for such characterization.

### Acknowledgements

This work was funded by the Midi-Pyrénées region and University of Toulouse. Mathias Destarac and COLCOM company are acknowledged for kindly providing PAPTAC-b-PNIPAM and DGL polymers respectively. Miss Hary Gassama is acknowledged for a short term help. SKRW and CRMB thank the National Science Foundation Grant CHE-1508827 for support.

### Appendix A. Supplementary data

Supplementary data associated with this article can be found, in the online version, at <http://dx.doi.org/10.1016/j.chroma.2016.12.050>.

### References

- [1] D.V. Pergushov, A.H.E. Muller, F.H. Schacher, Micellar interpolyelectrolyte complexes, *Chem. Soc. Rev.* 41 (2012) 6888–6901.
- [2] Y. Lee, K. Kataoka, Biosignal-sensitive polyion complex micelles for the delivery of biopharmaceuticals, *Soft Matter* 5 (2009) 3810–3817.
- [3] A. Harada, K. Kataoka, Effect of charged segment length on physicochemical properties of core-shell type polyion complex micelles from block ionomers, *Macromolecules* 36 (2003) 4995–5001.
- [4] P.S. Chelushkin, E.A. Lysenko, T.K. Bronich, A. Eisenberg, V.A. Kabanov, A.V. Kabanov, Polyion complex nanomaterials from block polyelectrolyte micelles and linear polyelectrolytes of opposite charge: 1. solution behavior, *J. Phys. Chem. B* 111 (2007) 8419–8425.
- [5] F. Maggi, S. Ciccarelli, M. Diociaiuti, S. Casciardi, G. Masci, Chitosan nanogels by template chemical cross-linking in polyion complex micelle nanoreactors, *Biomacromolecules* 12 (2011) 3499–3507.
- [6] J.-F. Gohy, S.K. Varshney, S. Antoun, R. Jérôme, Water-soluble complexes formed by sodium poly(4-styrenesulfonate) and a poly(2-vinylpyridinium)-block-poly(ethyleneoxide) copolymer, *Macromolecules* 33 (2000) 9298–9305.
- [7] S. De Santis, R. Diana Ladogana, M. Diociaiuti, G. Masci, Pegylated and thermosensitive polyion complex micelles by self-assembly of two oppositely and permanently charged diblock copolymers, *Macromolecules* 43 (2010) 1992–2001.
- [8] J. Warnant, N. Marcotte, J. Reboul, G. Layrac, A. Aqil, C. Jérôme, D.A. Lemer, C. Gérardin, Physicochemical properties of pH-controlled polyion complex (PIC) micelles of poly(acrylic acid)-based double hydrophilic block copolymers and various polyamines, *Anal. Bioanal. Chem.* 403 (2012) 1395–1404.
- [9] Y. Kakizawa, A. Harada, K. Kataoka, Environment-sensitive stabilization of core-shell structured polyion complex micelle by reversible cross-linking of the core through disulfide bond, *J. Am. Chem. Soc.* 121 (1999) 11247–11248.
- [10] S. Herlambang, M. Kumagai, T. Nomoto, S. Horie, S. Fukushima, M. Oba, K. Miyazaki, Y. Morimoto, N. Nishiyama, K. Kataoka, Disulfide crosslinked polyion complex micelles encapsulating dendrimer phthalocyanine directed to improved efficiency of photodynamic therapy, *J. Control. Release* 155 (2011) 449–457.
- [11] J. Wang, D. Zhao, Y. Wang, G. Wu, Imine bond cross-linked poly(ethylene glycol)-block-poly(aspartamide) complex micelle as a carrier to deliver anticancer drugs, *RSC Adv.* 4 (2014) 11244–11250.
- [12] J. Zhang, Y. Zhou, Z. Zhu, Z. Ge, S. Liu, Polyion complex micelles possessing thermoresponsive Coronas and their covalent core stabilization via click chemistry, *Macromolecules* 41 (2008) 1444–1454.
- [13] R. Ideta, F. Tasaka, W.-D. Jang, N. Nishiyama, G.-D. Zhang, A. Harada, Y. Yanagi, Y. Tamaki, T. Aida, K. Kataoka, Nanotechnology-based photodynamic therapy for neovascular disease using a supramolecular nanocarrier loaded with a dendritic photosensitizer, *Nano Lett.* 5 (2005) 2426–2431.
- [14] W.-D. Jang, N. Nishiyama, D. Zhang, A. Harada, D.-L. Jang, S. Kawauchi, Y. Morimoto, M. Kikuchi, H. Koyama, T. Aida, K. Kataoka, Supramolecular nanocarrier of anionic dendrimer porphyrins with cationic block copolymers modified with polyethyleneglycol to enhance intracellular photodynamic efficacy, *Angew. Chem. Int. Ed. Engl.* 44 (2005) 419–423.
- [15] W.-D. Jang, Y. Nakagishi, N. Nishiyama, S. Kawauchi, Y. Morimoto, M. Kikuchi, K. Kataoka, Polyion complex micelles for photodynamic therapy: incorporation of dendritic photosensitizer excitable at long wavelength relevant to improved tissue-penetrating property, *J. Control. Release* 113 (2006) 73–79.

- [16] H. Chen, L. Xiao, Y. Anraku, P. Mi, X. Liu, H. Cabral, A. Inoue, T. Nomoto, A. Kishimura, N. Nishiyama, K. Kataoka, Polyion complex vesicles for photoinduced intracellular delivery of amphiphilic photosensitizer, *J. Am. Chem. Soc.* 136 (2014) 157–163.
- [17] M. Dionzou, A. Morère, C. Roux, B. Lonetti, J.-D. Marty, C. Mingotaud, P. Joseph, D. Goudounèche, B. Payré, M. Léonetti, A.F. Mingotaud, Comparison of methods for the fabrication and the characterization of polymer self-assemblies: what are the important parameters? *Soft Matter* 12 (2016) 2166–2176.
- [18] J.P. Patterson, M.P. Robin, C. Chassenieux, O. Colombani, R.K. O'Reilly, The analysis of solution self-assembled polymeric nanomaterials, *Chem. Soc. Rev.* 43 (2014) 2412–2425.
- [19] A. Zattoni, B. Roda, F. Borghi, V. Marassi, P. Reschiglian, Flow field flow fractionation for the analysis of nanoparticles used in drug delivery, *J. Pharm. Biomed. Anal.* 87 (2014) 53–61.
- [20] C. Bria, F. Violleau, S.K.R. Williams, Field-flow fractionation for biological, natural, and synthetic polymers: recent advances and trends, *Lc Gc Asia Pacific* 16 (2013) 8–16.
- [21] L. Nilsson, Separation and characterization of food macromolecules using field-flow fractionation: a review, *Food Hydrocoll.* 30 (2013) 1–11.
- [22] F. von der Kammer, S. Legros, E.H. Larsen, K. Loeschner, T. Hofmann, Separation and characterization of nanoparticles in complex food and environmental samples by field-flow fractionation, *Trends Anal. Chem.* 30 (2011) 425–436.
- [23] M. Baalousha, B. Stolpe, J.R. Lead, Flow field-flow fractionation for the analysis and characterization of natural colloids and manufactured nanoparticles in environmental systems: a critical review, *J. Chromatogr. A* 1218 (2011) 4078–4103.
- [24] G. Yohannes, M. Jussila, K. Hartonen, M.L. Riekkola, Asymmetrical flow field-flow fractionation technique for separation and characterization of biopolymers and bioparticles, *J. Chromatogr. A* 1218 (2011) 4104–4116.
- [25] R.N. Qureshi, W.T. Kok, Application of flow field-flow fractionation for the characterization of macromolecules of biological interest: a review, *Anal. Bioanal. Chem.* 399 (2011) 1401–1411.
- [26] D.C. Rambaldi, P. Reschiglian, A. Zattoni, Flow field-flow fractionation: recent trends in protein analysis, *Anal. Bioanal. Chem.* 399 (2011) 1439–1447.
- [27] B. Roda, A. Zattoni, P. Reschiglian, M.H. Moon, M. Mirasoli, E. Micheline, A. Roda, Field-flow fractionation in bioanalysis: a review of recent trends, *Anal. Chim. Acta* 635 (2009) 132–143.
- [28] P. Reschiglian, M.H. Moon, Flow field-flow fractionation: a pre-analytical method for proteomics, *J. Proteom.* 71 (2008) 265–276.
- [29] W. Fraunhofer, G. Winter, The use of asymmetrical flow field-flow fractionation in pharmaceuticals and biopharmaceutics, *Eur. J. Pharm. Biopharm.* 58 (2004) 369–383.
- [30] M.-K. Liu, P.S. Williams, M.N. Myers, J.C. Giddings, Hydrodynamic relaxation in flow field-flow fractionation using both split and frit inlets, *Anal. Chem.* 63 (1991) 2115–2122.
- [31] J.C. Giddings, Hydrodynamic relaxation and sample concentration in field-flow fractionation using permeable wall elements, *Anal. Chem.* 62 (1990) 2306–2312.
- [32] M.-K. Liu, P. Li, J.C. Giddings, Rapid protein separation and diffusion coefficient measurement by frit inlet flow field-flow fractionation, *Protein Sci.* 2 (1993) 1520–1531.
- [33] M.H. Moon, Frit-inlet asymmetrical flow field-flow fractionation: a stopless separation technique for the separation of macromolecules and nanoparticles, *Bull. Korean Chem. Soc.* 22 (2001) 337–348.
- [34] M.H. Moon, P.S. Williams, H. Kwon, Retention and efficiency in frit inlet asymmetrical flow field-flow fractionation (FIA-FIFFF), *Anal. Chem.* 71 (1999) 2957–2966.
- [35] M.H. Moon, H. Kwon, I. Park, Stopless flow injection in asymmetrical flow field-flow fractionation using a frit inlet, *Anal. Chem.* 69 (1997) 1436–1440.
- [36] M.H. Moon, H. Kwon, I. Park, Stopless separation of proteins by frit-inlet asymmetrical flow field-flow fractionation, *J. Liq. Chromatogr. Relat. Technol.* 20 (1997) 2803–2814.
- [37] M.H. Moon, J. Lee, J. Park, Effect of inlet frit lengths in the hydrodynamic relaxation efficiency in frit inlet asymmetrical flow field flow fractionation, *J. Liq. Chromatogr. Relat. Technol.* 26 (2003) 2369–2379.
- [38] D. Kang, M.H. Moon, Miniaturization of frit inlet asymmetrical flow field-flow fractionation, *Anal. Chem.* 76 (2004).
- [39] M.H. Moon, D. Kang, I. Hwang, P.S. Williams, Field and flow programming in frit-inlet asymmetrical flow field-flow fractionation, *J. Chromatogr. A* 955 (2002) 263–272.
- [40] I. Park, K.-J. Paeng, Y. Yoon, J.-H. Song, M.H. Moon, Separation and selective detection of lipoprotein particles of patients with Coronary artery disease by frit-inlet asymmetrical flow field-flow fractionation, *J. Chromatogr. B* 780 (2002) 415–422.
- [41] M.H. Moon, D. Kang, K. Jung, J. Kim, Separation of carbon nanotubes by frit inlet asymmetrical field-flow fractionation, *J. Sep. Sci.* 27 (2004) 710–717.
- [42] H. Lee, H. Kim, M.H. Moon, Field programming in frit inlet asymmetrical flow field-flow fractionation/multiangle light scattering: application to sodium hyaluronate, *J. Chromatogr. A* 1089 (2005) 203–210.
- [43] H. Kim, H. Lee, M.H. Moon, Size characterization of sodium hyaluronate by field programming frit inlet asymmetrical flow field-flow fractionation/multiangle light scattering, *Bull. Korean Chem. Soc.* 27 (2006) 413–418.
- [44] M. Ali, E. Hwang, I.-H. Cho, M.H. Moon, Characterization of sodium hyaluronate blends using frit inlet asymmetrical flow field-flow fractionation & multiangle light scattering, *Anal. Bioanal. Chem.* 402 (2012) 1269–1276.
- [45] S. Woo, J.W. Lee, W. Choi, M.H. Moon, Characterization of ultrahigh molecular weight cationic polyacrylamide by frit-inlet asymmetrical flow field-flow fractionation and multiangle light scattering, *J. Chromatogr. A* 1429 (2016) 304–310.
- [46] K. Knop, A.F. Mingotaud, N. El-Akra, F. Violleau, J.P. Souchard, Monomeric micellorhizide(a)-containing poly(ethylene glycol)-b-epsilon-caprolactone) block copolymer for photodynamic therapy, *Photochem. Photobiol. Sci.* 8 (2009) 396–404.
- [47] J. Ehrhart, A.-F. Mingotaud, F. Violleau, Asymmetrical flow field-flow fractionation with multi-angle light scattering and quasi elastic light scattering for characterization of poly(ethylene glycol)-b-epsilon-caprolactone) block copolymer self-assemblies used as drug carriers for photodynamic therapy, *J. Chromatogr. A* 1218 (2011) 4249–4256.
- [48] L. Gibot, A. Lemelle, U. Till, B. Moukarzel, A.F. Mingotaud, V. Pimienta, P. Saint-Aguet, M.P. Rols, M. Gaucher, F. Violleau, C. Chassenieux, P. Vicendo, Polymeric micelles encapsulating photosensitizer: structure/photodynamic therapy efficiency relation, *Biomacromolecules* 15 (2014) 1443–1455.
- [49] U. Till, M. Gaucher-Delmas, P. Saint-Aguet, G. Hamon, J.-D. Marty, C. Chassenieux, B. Payré, D. Goudounèche, A.F. Mingotaud, F. Violleau, Asymmetrical flow field-flow fractionation with multi-angle light scattering and quasi elastic light scattering for characterization of polymerosomes: comparison with classical techniques, *Anal. Bioanal. Chem.* 406 (2014) 7841–7853.
- [50] D. Le Cerf, S. Simon, J.-F. Argillier, L. Picton, Contribution of flow field flow fractionation with on line static and dynamic light scattering to the study of hydrocolloidal polyelectrolyte complexes, *Anal. Chim. Acta* 604 (2007) 2–8.
- [51] D. Le Cerf, A.S. Pepin, P.M. Niang, M. Cristea, C. Karakasyan-Dia, L. Picton, Formation of polyelectrolyte complexes with diethylaminoethyl dextran: charge ratio and molar mass effect, *Carbohydr. Polym.* 113 (2014) 217–224.
- [52] G. Yohannes, S. Holappa, S.K. Wiedmer, T. Andersson, H. Tenhu, M.-L. Riekkola, Polyelectrolyte complexes of poly(methacryloxyethyl trimethylammonium chloride) and poly(ethylene oxide)-block-poly(sodium methacrylate) studied by asymmetrical flow field-flow fractionation and dynamic light scattering, *Anal. Chim. Acta* 542 (2005) 222–229.
- [53] A.T. Sutton, E. Read, A.R. Maniego, J.J. Thevarajah, J.-D. Marty, M. Destarac, M. Gaborieau, P. Castignolles, Purity of double hydrophilic block copolymers revealed by capillary electrophoresis in the critical conditions, *J. Chromatogr. A* 1372 (2014) 187–195.
- [54] K.G. Wahlund, Flow field-flow fractionation: critical overview, *J. Chromatogr. A* 1287 (2013) 97–112.
- [55] M. Schimpf, K. Caldwell, J.C. Giddings, *Field-Flow Fractionation Handbook*, John Wiley & Sons, New York, 2000.
- [56] R.L. Hartmann, S.K.R. Williams, Flow field-flow fractionation as an analytical technique to rapidly quantitate membrane fouling, *J. Membr. Sci.* 209 (2002) 93–106.
- [57] G.E. Kassalainien, S.K.R. Williams, Assessing protein-ultrafiltration membrane interactions using flow field-flow fractionation, in: S.K.R. Williams, K. Caldwell (Eds.), *Field-Flow Fractionation Biopolym. Anal.*, Springer-Verlag, Wien, 2012.
- [58] J. Ashby, S. Schachermer, Y. Duan, L.A. Jimenez, W. Zhong, Probing and quantifying DNA-protein interactions with asymmetrical flow field-flow fractionation, *J. Chromatogr. A* 1358 (2014) 217–224.
- [59] P. Li, M. Hansen, J.C. Giddings, Advances in frit-inlet and frit-outlet flow field-flow fractionation, *J. Microcolumn Sep.* 10 (1998) 7–18.
- [60] M.H. Moon, I. Hwang, Hydrodynamic vs. focusing relaxation in asymmetrical flow field-flow fractionation, *J. Liq. Chromatogr. Relat. Technol.* 24 (2001) 3069–3083.
- [61] A. Litzen, K.G. Wahlund, Zone broadening and dilution in rectangular and trapezoidal asymmetrical flow field-flow fractionation channels, *Anal. Chem.* 63 (1991) 1001–1007.
- [62] J. Li, W.-D. He, N. He, S.-C. Han, X.-L. Sun, L.-Y. Li, B.-Y. Zhang, Synthesis of PEG-PNIPAM-Plys hetero-arm star polymer and its variation of thermo-responsibility after the formation of polyelectrolyte complex micelles with PAA, *J. Polym. Sci. A: Polym. Chem.* 47 (2009) 1450–1462.
- [63] A. Harada, K. Kataoka, Novel polyion complex micelles entrapping enzyme molecules in the core. 2. Characterization of the micelles prepared at nonstoichiometric mixing ratios, *Langmuir* 15 (1999) 4208–4212.
- [64] A. Harada, K. Kataoka, Novel polyion complex micelles entrapping enzyme molecules in the Core: preparation of narrowly-distributed micelles from lysozyme and poly(ethylene glycol)-poly(aspartic acid) block copolymer in aqueous medium, *Macromolecules* 31 (1998) 288–294.
- [65] A. Harada, K. Kataoka, Switching by pulse electric field of the elevated enzymatic reaction in the core of polyion complex micelles, *J. Am. Chem. Soc.* 125 (2003) 15306–15307.
- [66] R. Ma, B. Wang, X. Liu, Y. An, Y. Li, Z. He, L. Shi, Pyranine-induced micellization of poly(ethylene glycol)-block-poly(4-vinylpyridine) and pH-triggered release of pyranine from the complex micelles, *Langmuir* 23 (2007) 7498–7504.
- [67] S.-i. Yusa, Y. Yokoyama, Y. Morishima, Synthesis of oppositely charged block copolymers of poly(ethylene glycol) via reversible addition-fragmentation chain transfer radical polymerization and characterization of their polyion complex micelles in water, *Macromolecules* 42 (2009) 376–383.
- [68] W. Burchard, *Static and Dynamic Light Scattering from Branched Polymers and Biopolymers*, Light Scattering from Polymers, Springer Berlin Heidelberg, Berlin, Heidelberg, 1983, pp. 1–124.